A R C H I V E S O F M E T A L L U R G Y A N D M A T E R I A L S
Volume 50 2005 Issue 2

M.J. ZEHETBAUER*, E. SCHAFLER*, T. UNGAR**

QUANTIFICATION OF NANOCRYSTALLIZATION BY MEANS OF X-RAY LINE PROFILE ANALYSIS[1)]

ILOŚCIOWY OPIS NANOKRYSTALICZNOŚCI PRZY UŻYCIU ANALIZY PROFILU LINII RENTGENOWSKIEJ

In crystalline materials the structural scale reaches submicron or even nanometer sizes when plastic deformation is sustained up to very high strains, low deformation temperatures and/or extended hydrostatic pressure. In order to find out the mechanisms of crystal fragmentation, X-ray Line Profile Analysis (XPA) can provide a number of important parameters which are not (or only scarcely) available by other methods such as TEM and residual electrical resistivity. These are the density, arrangement and type of dislocations, and the internal stresses which all can be determined even in case of very large strains and high contents of alloying atoms. Extending XPA to profiles at high order diffraction (Multi Reflection Profile Analysis, MXPA) it is possible to carefully separate strain broadening from size broadening. This is particularly important when the nanomaterials reveal grain sizes smaller than 100 nm, when the size broadening gets similarly high than strain broadening from plastic deformation. In dislocated metals, the dislocation contrast has to be taken into account for a correct evaluation of grain size which reduces to the coherently scattering domain size in case of nanocrystallization due to plastic deformation, namely SPD. When using highly intense Synchrotron radiation, a maximum in spatial and even time resolution is reached enabling in-situ measurements during deformation of the parameters quoted.
Keywords: Multi Reflection Profile Analysis, Size and Strain Broadening, Nanocrystallization, Severe Plastic Deformation, Synchrotron radiation

W materiałach polikrystalicznych bardzo silnie odkształconych plastycznie przy niskich temperaturach i w warunkach ciśnienia hydrostatycznego, skala badań strukturalnych osiąga rozmiary sub- lub nanometryczne. Analiza profilu linii rentgenowskiej (XPA) może dostarczyć wielu ważnych informacji o mechanizmach fragmentacji kryształów, nieosiągalnych w ogóle (lub tylko w ograniczonym zakresie) innymi metodami, jak np. TEM czy elektryczna oporność właściwa. Nawet w przypadku bardzo dużych odkształceń i dużej zawartości

* MATERIALS PHYSICS INSTITUTE, UNIVERSITY OF VIENNA, AUSTRIA
** DEPARTMENT OF GENERAL PHYSICS, EOTVOS UNIVERSITY BUDAPEST, HUNGARY
1) invited lecture

dodatków stopowych, możliwe jest określenie gęstości i typu dyslokacji sieciowych oraz naprężeń własnych.

Rozszerzając analizę XPA na odbicia dyfrakcyjne wyższych rzędów (Multi Reflection Profile Analysis, MXPA) możliwe jest rozdzielenie wpływu odkształcenia oraz rozdrobnienia ziarna na poszerzenie profilu. Jest to szczególnie ważne w przypadku nanomateriałów cechujących się rozmiarem ziaren mniejszym niż 100 nm, kiedy to wpływ rozdrobnienia ziarna na poszerzenie profilu staje się porównywalny w wpływem deformacji plastycznej.

W materiałach o dużej gęstości dyslokacji (np. po procesie SPD), poprawna ocena wielkości ziarna wymaga uwzględnienia kontrastu dyslokacyjnego, który redukuje ją do rozmiaru obszarów spójnego rozpraszania. Stosując intensywne promieniowanie synchrotronowe, można osiągnąć znaczną rozdzielczość przestrzenną oraz czasową, co pozwala na pomiary in-situ podczas odkształcenia, a tym samym umożliwia ocenę parametrów deformacji.

1. Introduction

From strong definition, nanocrystalline materials reveal a microstructure of a characteristic length scale of up to a few tens of nanometers far off from thermodynamic equilibrium. This range may be extended up to a few hundreds of nanometers (also called "ultrafine grained" or "submicron" materials) because such materials still reveal properties of genuine nanocrystalline materials which deviate from those of single crystal and/or coarse-grained polycrystals, in a characteristic way. In fact, nanomaterials in the wider definition exhibit particular mechanical, magnetic, electronic and other physical properties. While the mechanical properties include enhanced strength sometimes in parallel with increased ductility, the magnetic properties are distinguished by enhanced coercive force of isotropic hard magnetic materials or minimisation of hysteresis losses in soft magnetic materials, in order to quote some important examples. In general, nanocrystalline materials can be produced by two different ways:

(i) By "***bottom-up***" methods (inert gas condensation [1], electrodeposition [2], consolidation of powders [3] , crystallization from amorphous materials [4], or

(i) by "*top-down*" methods (shock wave loading [5], Severe Plastic Deformation (SPD) [6, 7]).

"Bottom-up" methods like those of inert gas condensation and electrodeposition provide materials with very small grain sizes down to a few nanometers while the sample dimensions are limited. However, often porosity occurs and impurities are introduced as in case of consolidated powders, strongly deteriorating the good mechanical properties. "Top-down" methods can yield compact non-porous material, where primarily *Severe Plastic Deformation (SPD)* is of highest technological interest because of its potential to achieve bulk shape nanomaterials. SPD is described as "intense plastic straining under high imposed pressure" [8]. The hydrostatic pressure is built up by a constraint during deformation. Although there exists various methods of SPD which can be classified by their strain paths, the constraint is common with all of them. In case of the so-called "Equal Channel Angular Extrusion (ECAE)" [9-11] (Fig. 1a), the "Twist Extrusion (TE)" [12, 13] (Fig. 1b) or the Cyclic Extrusion Compression (CEC)

[14, 15] (Fig. 1d) this constraint is acting across the deformation axis, while with the "High Pressure Torsion (HPT)" [10, 16-18] (Fig. 1c) all the sample is underlying this constraint. In case of HPT the constraint can be systematically controlled by applying certain levels of hydrostatic pressure during the deformation by torsion. As a significant feature of SPD, it is the magnitude of hydrostatic pressure which governs the extent of the achievable strain as well as the resulting grain size, the strength and the ductility of the material related [19].

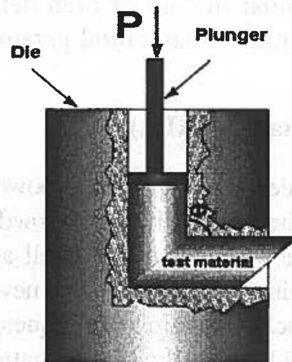

Fig. 1(a)

Fig. 1(b)

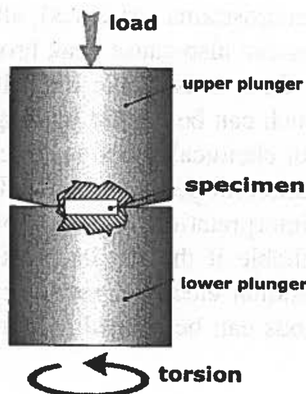

Fig. 1(c)

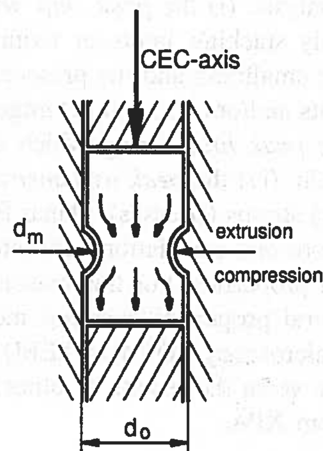

Fig. 1(d)

Fig. 1. Different deformation modes of Severe Plastic Deformation all exhibiting the presence of a certain constraint. (a) Equal Channel Angular Pressing (ECAP), (b) Twist Extrusion, (c) High Pressure Torsion, (d) Cyclic Extrusion Compression (for references, see text)

Be it from bottom-up or top down methods, the size and/or the parameters of nanostructure within the grains are strictly determining the properties of nanomaterials. This paper is to show how the X-ray diffraction line profile analysis (XPA) is capable of determining both i.e. not only the coherently scattering domain size but also the nature, density and distributions of lattice defects such as dislocations, planar faults and even point defects. In this sense, the XPA has been developed to a serious alternative to scanning and transmission electron microscopy methods, or has been even exhibiting clear advantages as concerns its measuring potential in case of high defect densities as well as its capability of in-situ deformation studies of structural parameters.

2. X-ray Line Profile Analysis (XPA)

The X-ray line profile analysis (XPA) has been developed to a powerful tool for the characterisation of microstructures either in the bulk or in loose powder materials. During the last years, the modelling and evaluation procedures as well as the experimental possibilities and techniques have been gradually improved. The new generations of X-ray generators, enhanced focusing and monochromatizing techniques, and last not least the usage of the high brilliant synchrotron radiation allow investigations in highly plastically deformed materials, and with high resolution in time and space, respectively.

The ideal diffraction pattern consists of narrow, symmetrical, delta-function like peaks, positioned according to a well defined unit cell. Numerous deviations from the ideal pattern are related to the microstructure of the material and are the subject of peak profile analysis: (i) the *peak shift* which is related to internal stresses or planar faults, especially stacking faults or twinning; (ii) the *peak broadening* which indicates crystallite smallness and the presence of microstrains (-stresses), although strain (stress) gradients and/or chemical heterogeneities can also cause peak broadening; (iii) the *anisotropic peak broadening* which arises from anisotropic crystallite shape or anisotropic strain. (iv) the *peak asymmetries* which can be caused by long-range internal (third order) strains (stresses), planar faults or chemical heterogeneities. In general, there is no one-to-one correlation between the different peak profiles and the different microstructural properties. For this reason the interpretation of peak profiles in terms of microstructural properties becomes more reliable if the results of other methods, e.g. electron microscopy (TEM or SEM) or residual electrical resistivity (RER), are also used. Vice versa the results of other methods can be refined and/or amended by using those from XPA.

Strain broadening

According to the kinematical theory of scattering, diffraction profiles are the convolution of the size (S) and distortion (D) profiles. The Fourier transform of this is the Warren-Averbach equation [20]

$$A(L) = A^S(L)A^D(L) \quad (1)$$

in terms of Fourier coefficients A^i(L), L being the Fourier length. This equation has a wide generality and has been theoretically verified by several authors individually. One of the main challenge related to this equation is the way in which the size Fourier coefficients, A^S(L), and the mean square strain, $<\varepsilon_{g,L}{}^2>$, are interpreted (g is the length of diffraction vector).

Numerous experiments have shown that the mean square strain does always depend on g as well as L [21, 22]. Theoretical models accounting for different types of lattice defects (Wilkens, Krivoglaz and others [23, 24]) have been applied to the experimentally observed behaviour of the mean square strain. It turned out that the major contribution of strain to diffraction peak broadening comes from dislocations.

The g — dependence of the mean square strain is known in powder diffraction as "strain anisotropy" [25]. This means that neither the width nor the Fourier coefficients of the diffraction profiles are monotonic functions of the diffraction angle. Two in principle different approaches have been developed so far for the interpretation of strain anisotropy: (i) a phenomenological model based on the anisotropy of the elastic properties of crystals [21], and (ii) the dislocation model based on the mean square strain of dislocated crystals [22]. The dislocation model of $<\varepsilon_{L,g}{}^2>$ takes into account that the contribution of singular dislocation to strain broadening depends on the relative orientations between the diffraction vector **g**, and the line and Burgers vectors of dislocations, **l** and **b**, respectively, in a similar way as the contrast of dislocations in electron microscopy. The anisotropic contrast can be described by contrast factors, C, which can be calculated numerically on the basis of the crystallography of dislocations and the elastic constants of the crystal [23, 26-28]. In the case of a texture free polycrystal, of a loose powder sample, and/or a random population of all possible Burgers vectors, the individual contrast factors can be averaged over the permutations of the hkl indices. It can be shown that the average contrast factor, $\overline{C}$, is a linear function of the fourth order invariants of the hkl indices [29]. In the case of cubic and hexagonal crystals this can be written as:

$$\overline{C} = \overline{C}_{h00}(1 - qH^2) \text{ and } \overline{C}_{hk.l} = \overline{C}_{hk.0}[1 + q_1 x + q_2 x^2], \quad (2)$$

respectively, where $\overline{C}_{h00}$ and $\overline{C}_{hk0}$ are the average dislocation contrast factors for the $h00$ and $hk0$ reflections, respectively, $H^2 = (h^2k^2+h^2l^2+k^2l^2)/(h^2+k^2+l^2)^2$; q, q_1 and q_2 are parameters depending on the elastic constants and on the character of dislocations in the crystal (e.g. edge or screw, or basal, prismatic or pyramidal, respectively). In the case of hexagonal crystals, $x = (2/3)(l/ga)^2$ in eq. (2) where l and a are the prismatic index and the basal lattice constant, respectively. Detailed accounts and compilations of the q, q_1 and q_2 parameters can be found in [27, 28]. A phenomenological interpretation of anisotropic strain broadening has been given by Stokes and Wilson [30] and Stephens [31].

Recently the theoretical framework for strain evaluation by means of MXPA has been further improved by Ungar et al. [22] by taking into consideration the influences of stacking faults to the Bragg profile which have been described in detail by Warren

[32]. In principle this opens the possibility to determine the density of stacking faults in addition to that of dislocations.

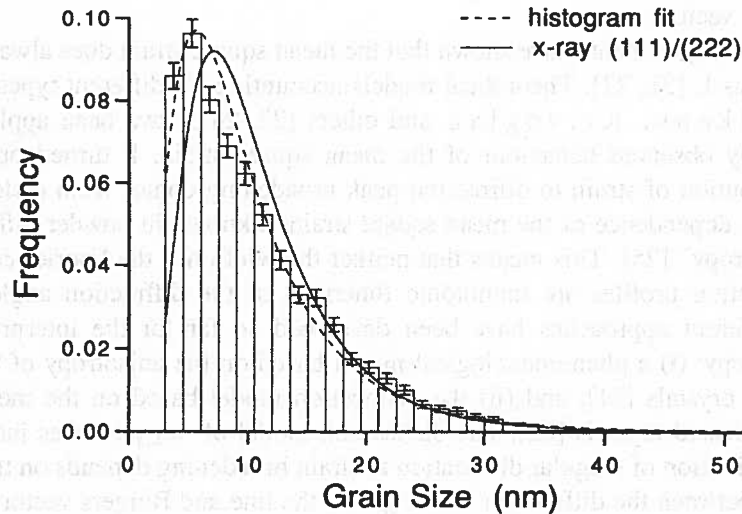

Fig. 2. Crystallite size distribution of nanocrystalline Pd produced by inert gas condensation and subsequent consolidation. The histogram fit (dashed line) connects data from TEM, the other fit (full line) connects data from X-ray line profile analysis being evaluated with the classical Warren- Averbach method [20]

Size broadening

Size broadened profiles can be described by assuming (i) a size distribution function and (ii) the shape of crystallites, or coherently scattering domains. Krill and Birringer [33] showed that the crystallite size distribution of nanocrystalline Pd produced by inert gas condensation and subsequent consolidation can be described by a log-normal size distribution function $f(x)$, given by the median m and the variance σ. Here the 111/222 pair of X-ray diffraction peaks were evaluated by the classical Warren-Averbach method [20]. Fig. 2 demonstrates the excellent correlation of the size distribution determined by transmission electron microscopy and by X-ray line profile analysis. For a log-normal distribution Hinds [34] has shown that the arithmetic-, the area- and the volume weighted average crystallite diameters are given by

$$< x >_k = m \exp(k\sigma^2), \quad (3)$$

where k = 0.5, 2.5 and 3.5 in the case of arithmetic-, area- and volume weighted averages.

Peak asymmetry

The peak asymmetries indicate the presence of long-range internal stresses, in correspondence with the composite model describing the heterogeneous dislocation distribution in terms of dislocation poor (cell interiors) and dislocation rich (cell walls) regions [35]. The hard cell wall- and the soft cell-interior materials are put under the forward and backward long-range internal stresses alternating concomitantly with the spatial variation of high and low dislocation densities. The spatial variation of the long-range internal stresses e.g. imposes a spatially varying tetragonal distortion on the cubic lattice of copper. The peak asymmetry is the manifestation of this varying tetragonality. The evaluation method of the long-range internal stresses which is based on the composite model makes use of the whole profile description of dislocated crystals [36].

The evaluation procedure

A numerical evaluation procedure has been worked out which provides five or six physical parameters in the case of cubic, or hexagonal crystals, respectively [37]. In cubic crystals these parameters are: (i) the mean m, and (ii) the variance σ of the log-normal size distribution function, (iii) the dislocation density ρ, (iv) the dislocation arrangement parameter, $M = R_e\sqrt{\rho}$ (with R_e as the outer cut-off radius of the dislocation strain field), and (v) the q parameter being part of the dislocation contrast factor (eq. (2)).In case of hexagonal crystals, two q parameters (q_1 and q_2) represent the dislocation contrast, according to eq. (2).

The procedure consists in the following steps: (*a*) At first, the Fourier coefficients of the measured physical profiles are calculated by means of a non-equidistant sampling Fourier transformation, (*b*) the Fourier coefficients of the size and strain profiles are evaluated, (*c*) the experimental and the calculated Fourier coefficients are compared using the Marquardt- Levenberg [38, 39] least squares procedure [37].

3. Application of Multiple X-Ray Profile Analysis to Nanocrystallization

Nanostructure in ED Ni. Electrodeposited (ED) nanocrystalline Ni foils were produced by pulse plating onto titanium substrate [40]. Six reflections were measured and the standard Williamson-Hall method has been applied [20, 41]. Fig. 3a shows the non- monotonic increase of the broadening with increasing absolute value of the diffraction vector. The increase indicates microstrains already being present in the as-produced sample. The non-monotonic behaviour can be ascribed to the particular contrast conditions. Extrapolating without contrast correction to K = 0 a value for the average crystallite size of 90 nm results. Afterwards the modified Williamson-Hall approach [21] has been applied to account for the strain anisotropy in terms of dislocation contrast, and the resulting plot, i.e. ΔK vs. $K.C^{1/2}$, has shown up markedly less scattering. A continuously monotonic curve has been received when the influences

of planar faults described above have been considered for the evaluation of measured profiles, too (Fig. 3b). Such faults are well known to grow during the ED process. Now a particle size of 50 nm resulted from MXPA evaluation which is markedly different from the size evaluation without contrast correction but in good correspondence with findings from TEM [40]. The average density of dislocations was 4.9×10^{15} m^{-2}, and most probably these are also grown-in defects formed during the deposition procedure. Under the assumption that during the ED process the planar faults are twin boundaries, the frequency of the latter is obtained as $\alpha = 0.0012$.

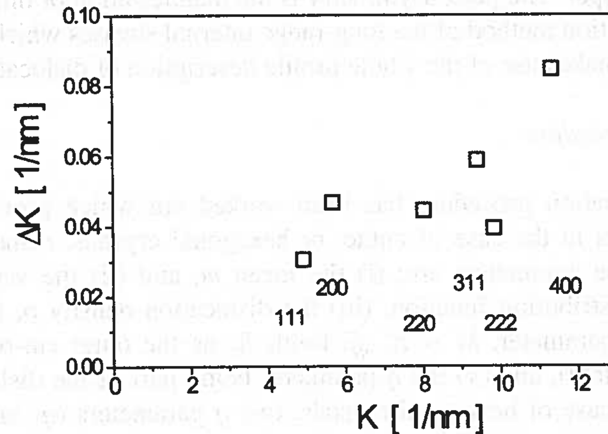

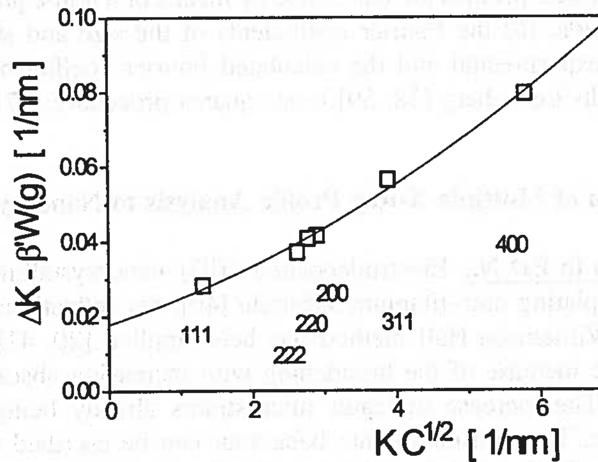

Fig. 3. Broadening of diffraction profiles measured in ED nanocrystalline Ni foils. (a) Standard Williamson-Hall plot; resulting crystallite size: 90 nm; (b) modified Williamson-Hall plot taking into account contrasts from dislocations as well as from stacking faults; resulting crystallite size: 50 nm

Nanostructures in SPD deformed Cu. Even more than in ED nanometals, the careful analysis of peak broadening in terms of a strain and a size effect is necessary to be applied for SPD nanometals, mostly because of the numerous lattice defects and local strains left within the grains after plastic deformation. A good example to what extent MXPA measurements can help to clarify e.g. strengthening mechanisms in SPD nanometals, is the investigation done by the authors in high pressure torsioned (HPT) Cu. These revealed ***coherently scattering domain sizes (CDSs)*** to be much smaller than grain sizes, especially in case of high hydrostatic pressure applied. Combined with a thorough investigation of microhardness (HV) as a function of torsional strain, it has been shown that, independent of the hydrostatic pressure applied, there is a clear relation between the CDS and the strength $\sigma \equiv HV/3$. This is seen from Fig. 4a which shows the strain dependent evolution of σ, the CDS, and the long range internal stresses as determined by the analysis of X-ray line profiles [42]; again, six reflections have been used for the evaluation. The inverse behaviour of σ and CDS suggested to draw a Hall-Petch type plot from which an exponent n = (-1) turned out to fit best the experimental results (Fig. 4b). The obvious change of slopes corresponds to the transition between deformation stages IV and V [42].

The same MXPA investigation yielded even two more important quantities: Besides the CDS, these are the ***long range internal stresses*** arising from the particular arrangements of dislocations. With increasing strain of HPT Cu, they grow to a maximum value of about 140 MPa, and then markedly decrease. This fact explains why — from a certain minimum strain — nanostructured HPT Cu exhibits not only an enhanced strength but also a gradually increasing ductility which appears as a paradoxon of classical metallurgy. The decrease of the internal stresses indicates a stress minimizing reorganisation of the dislocations in the grain interiors achieving a recovered and thus rehardenable nanostructure with much increased hardening coefficient thus providing a considerable ductility. This recovery effect may be a static one which is launched *after* deformation, i.e. during unloading under release of the hydrostatic pressure, or a dynamic one running *during* the continued torsion experiment [43]. Most probably both types of processes are contributing to the enhancement of deformability [43].

A third important quantity is the ***dislocation density*** involved in HPT Cu. In the authors' paper quoted above, dislocation densities have been determined by the MXPA method, too. Fig. 4c shows that the dislocation density not only depends on the strain but clearly also on the hydrostatic pressure applied. Recently, Zehetbauer et al [19] have adapted the large strain work hardening model of Zehetbauer [44, 45] to cases of extended hydrostatic pressure being present during deformation. With this model it was possible to simulate the dependence of dislocation density on hydrostatic pressure p (see the full lines in Fig. 4c), by adding p to the vacancy migration enthalpy [19]: So the effective migration enthalpy increases with hydrostatic pressure being present, which increasingly *impedes* the diffusion of vacancies and, due to the lack in vacancies, leads to a decrease of climbing of edge dislocations and thus to a decrease of edge dislocation annihilation. Thus, sufficient edge dislocations are available for constituting as many as grain boundaries being necessary for a formation of a real nanograin structure.

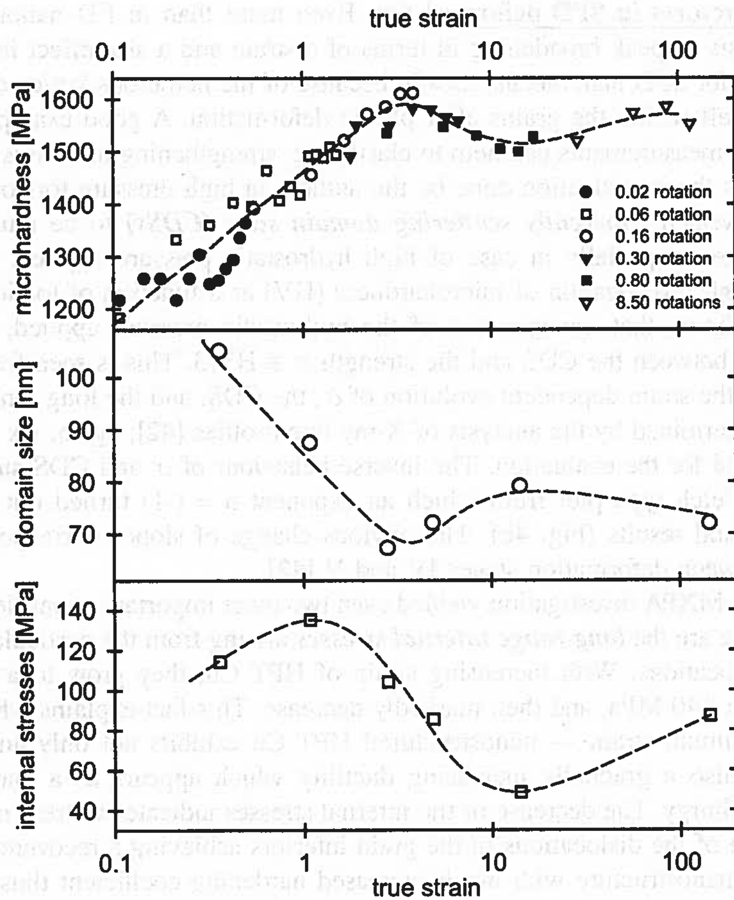

Fig. 4 (a)

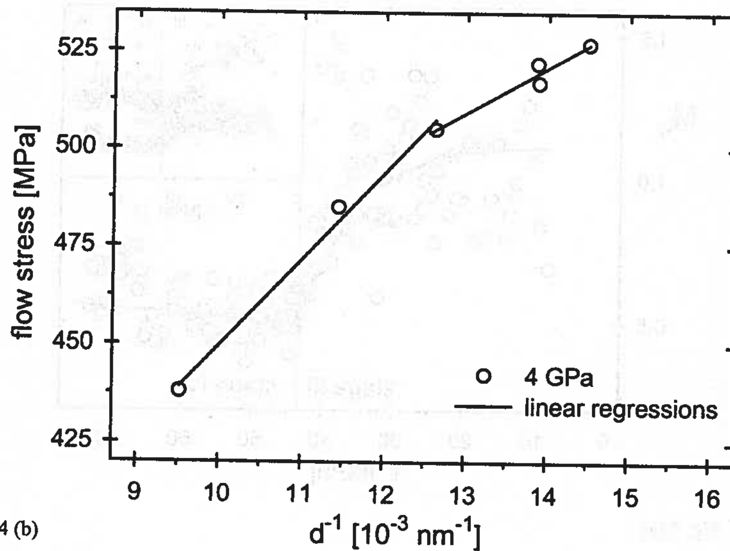

Fig. 4 (b)

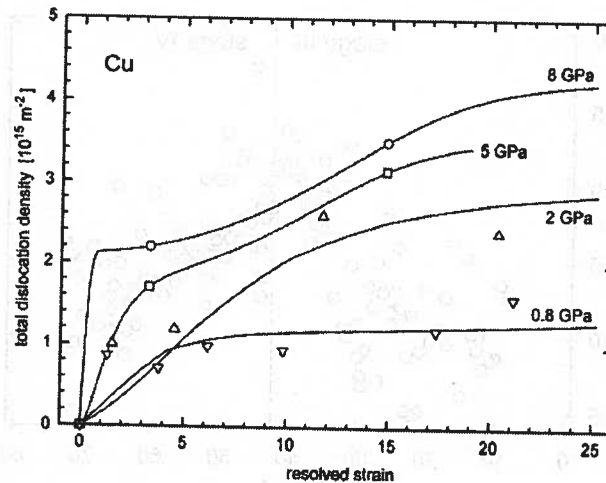

Fig. 4(c)

Fig. 4. Features of HPT Cu which has been deformed at an hydrostatic pressure of p = GPa to ultra-high strains at room temperature. (a) Inverse behaviour of microhardness, and the coherently scattering domain size (CDS) as measured by MXPA. The local internal stresses shown in the lowest graph indicate recovery effects going on with softening as reflected by the characteristics of microhardness. (b) Hall-Petch type plot suggesting an exponent of n = (-1) for the CDS. (c) Dislocation density measured by MXPA as a function of resolved shear strain. Applying an increasing level of hydrostatic pressure (values given as labels to the curves), increasing values of dislocation densities are observed

Time and Space Resolved Investigations of Nanocrystallisation. The analysis of the deformation induced fragmentation of materials by X-ray Bragg Profile Analysis

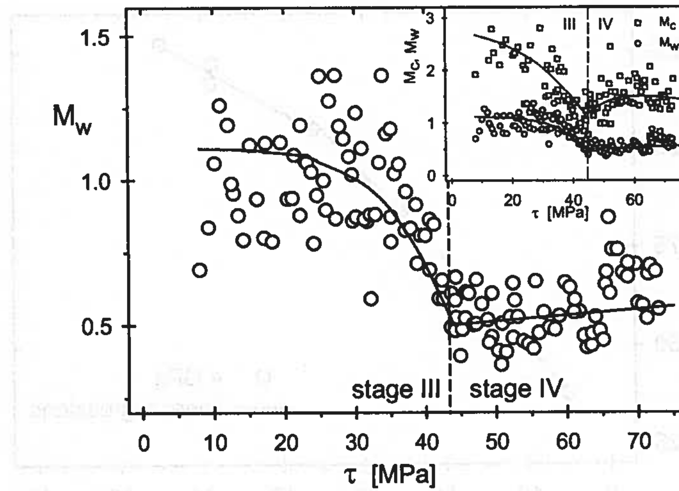

Fig. 5 (a)

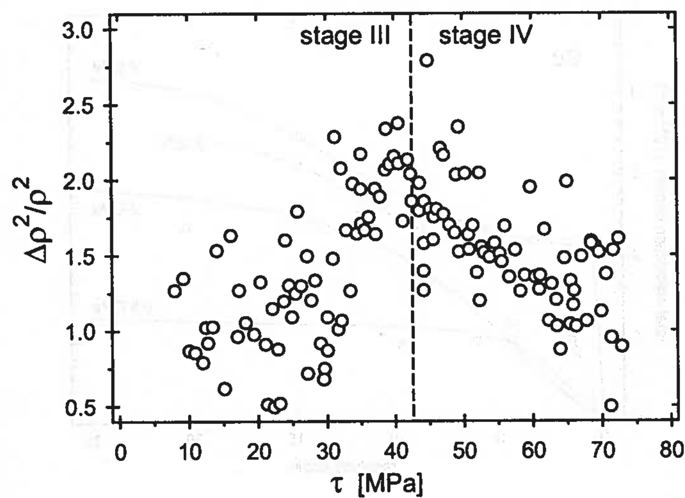

Fig. 5 (b)

Fig. 5. Features of second order type transition from cell boundary structure to grain boundary structure, reflected by (a) the minimum of dislocation arrangement parameter M_W of cell/grain boundaries as a function of resolved shear stress τ (M_C means the dislocation arrangement parameter in the cell/grain interiors and is shown for comparison in the insert) (b) the maximum of the square of the fluctuations of the dislocation density $\Delta\rho^2/\rho^2$ as a function of resolved shear stress ρ

is not restricted to the characterisation of severely plastically deformed materials. It is known that the formation of cells already starts at small amounts of deformation

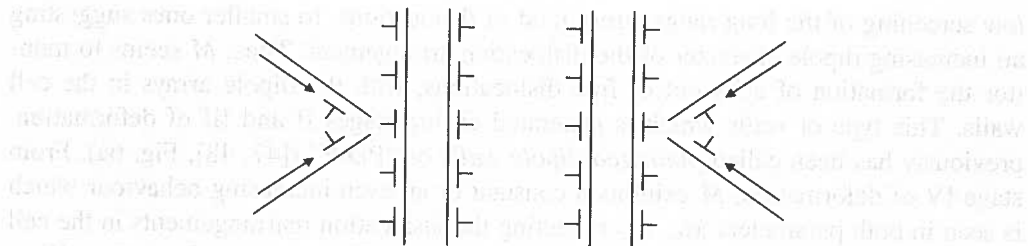

Fig. 6 (a)

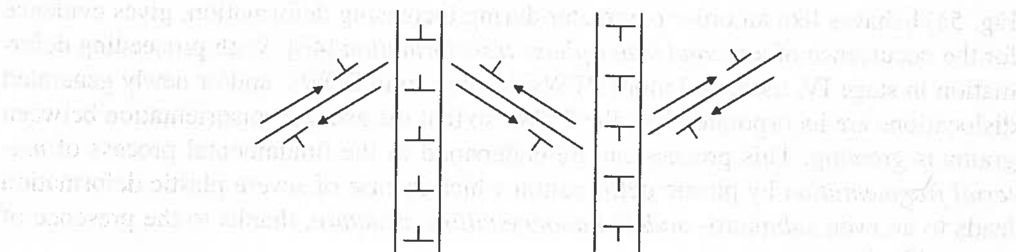

Fig. 6 (b)

Fig. 6. Sketches of the (a) Polarized Dipole Wall (PDW) structure, with no or slight misorientation between neighbouring areas ("cells") (b) Polarized Tilt Wall (PTW) structure, with marked misorientation between neighbouring areas ("grains")

regardless of conditions of temperature and hydrostatic pressure. At best the formation and the evolution of the dislocation cell structure can be investigated in a single crystal oriented for ideal multiple slip, by an in-situ experiment using synchrotron radiation which allows the fast but still careful measurement of Bragg profiles *in – situ* during deformation [46]. For the case of compression of [100] single crystals of Cu, Fig. 5a presents the evolution of the dislocation arrangement parameter M, as function of the applied stress. With proceeding deformation, M decreases from large values indicating

low screening of the long range stress field of dislocations, to smaller ones suggesting an increasing dipole character of the dislocation arrangement. Thus, M seems to monitor the formation of cells out of free dislocations, with the dipole arrays in the cell walls. This type of walls which is generated during stages II and III of deformation, previously has been called *polarized dipole walls* or "PDW" ([47, 48], Fig. 6a). From stage IV of deformation, M exhibits a constant or an even increasing behaviour which is seen in both parameters M_w, M_c reflecting the dislocation rearrangements in the cell walls and cell interiors, respectively (insert in Fig. 5a).The transition from stage III to stage IV is illustrated best by the fluctuations of the dislocation density shown in Fig. 5b. These can be concluded in case of very high density of data which is only possible from an experiment using Synchrotron radiation [46]. Just at the transition from stage III to stage IV, the fluctuations show a distinct maximum which strongly confirms previous findings [47, 48] that the PDWs transform into a new type of boundaries, the so-called *polarized tilt walls* (PTW, Fig. 6b). This structure achieves a marked misorientation between neighbouring cells i.e. represents the *"birth" of new grains* out of the almost equally oriented cells. The peak of the fluctuations together with the fact that the dislocation arrangement parameter in the cell-wall region, M_w (insert in Fig. 5a) behaves like an order parameter during increasing deformation, gives evidence for the occurrence of a *second order phase transformation* [46]. With proceeding deformation in stage IV, more and more PTWs develop from PDWs, and/or newly generated dislocations are incorporated into the PTWs so that the average misorientation between grains is growing. This process can be understood as the fundamental process of *material fragmentation* by plastic deformation which in case of severe plastic deformation leads to an even *sub*micro- *and/or nanocrystalline structure*, thanks to the presence of elevated hydrostatic pressure.

When performing X-ray Profile Analyses with highly intense synchrotron radiation, the spatial evolution of fragmentation can be also measured thanks to high *lateral* resolution achieved. In several experiments by the authors [49] individual grains of polycrystalline specimens with different amounts of cold rolling deformation have been scanned laterally by a collimated X-ray beam with a diameter of about 20 μm. For the example of Cu [48], Fig. 7a shows the scan within a grain from a sample which has been deformed to a true strain of 0.086. Here the dislocation density, the arrangement parameter M as well as the long range internal stresses remain rather constant within the grain, only in the wake of the grain boundaries (vertical dashed lines) the dislocation density and the long range internal stresses are increased [48]. This is the situation during stage II and III of deformation dominated by the PDW regime. Reaching higher deformations, the cell wall transformation sets in which results in the occurrence of local maxima in the dislocation density, and minima and the internal stresses, respectively (Fig. 7b): The occurrence of these extrema corresponds to the formation of PTWs out of the PDWs, which are able to incorporate much more dislocations as the screening of the dislocation strains is increased in this structure. The latter phenomenon is reflected by the local minima of M and of the internal stresses. With further deformation well into stage IV (Fig. 7c) more local maxima in the dislocation density appear in parallel

with minima of the internal stresses, indicating the continuing spread of PTW over all the microstructure leaving only a small number of PDW walls [48]. This means that the transformation of cell walls to grain boundaries is a gradual one, i.e. that it occurs during the whole stage IV of deformation connected with a continued increase of the strength. It should be noted, however, that the lateral resolution which could be reached by the use of Synchrotron is not better than about 5-20 μm which means that

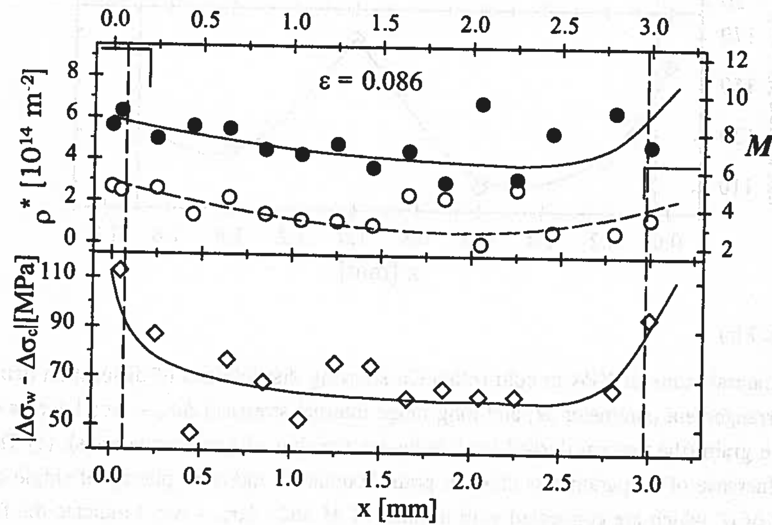

Fig. 7 (a)

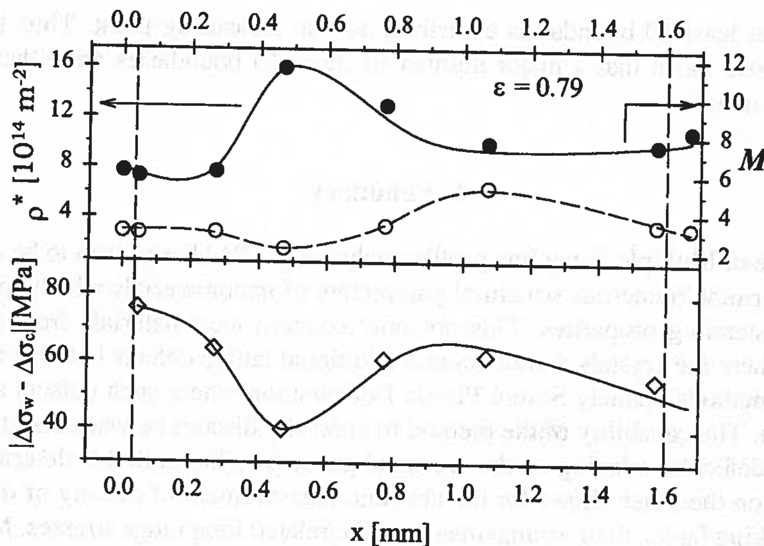

Fig. 7 (b)

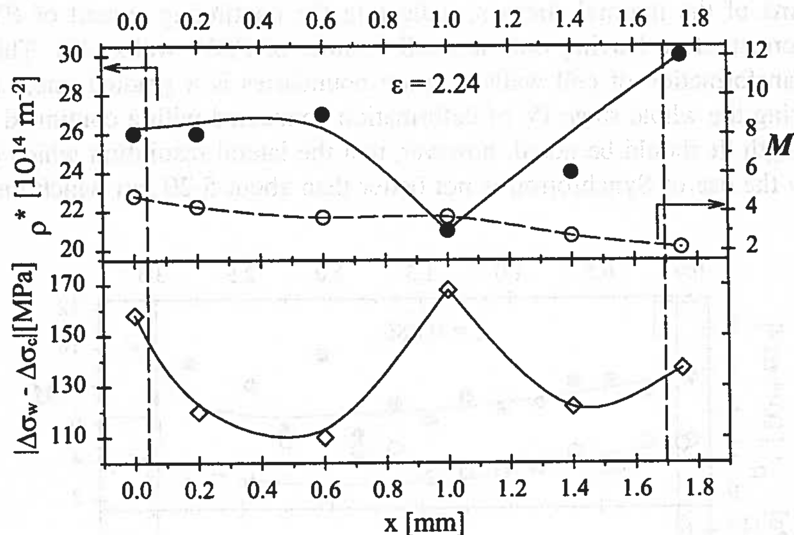

Fig. 7 (c)

Fig. 7. Lateral scans of XPA in cold-rolled Cu showing distributions of dislocation density ρ^*, dislocation arrangement parameter M, and long range internal stresses $|\Delta\sigma_w - \Delta\sigma_c|$ across the interiour of a single grain (the vertical dashed lines indicatee the sites of grain boundaries). (a) True strain $\varepsilon = 0.086$: Increase of all parameters close to grain boundaries indicates pile-up of single dislocations (b) Maxima of ρ^* which are connected with minima of M and $|\Delta\sigma_w - \Delta\sigma_c|$ indicate the formation of PTW-type boundaries (c) Minima of ρ^* which are connected with maxima of M and $|\Delta\sigma_w - \Delta\sigma_c|$ indicate some PDWs left in the grain interior which is dominated by the presence of PTWs

in average at least 10 boundaries contribute to one measuring point. Thus the results reported above mean that a major number of these 10 boundaries are either of PDW or of PTW nature.

4. Summary

The use of Multiple X-ray line profile analysis (MXPA) has proven to be a excellent tool to determine numerous structural parameters of nanomaterials which are essential for the outstanding properties. This not only concern nanomaterials from bottom-up methods where the crystals do not contain additional lattice defects but also those from top-down methods, namely Severe Plastic Deformation where such defects are present in the grain. The capability of the method to carefully discern between size broadening and lattice defect broadening on the one hand guarantees for a reliable determination of grain size, on the other allows for the absolute measurement of density of dislocations and/or stacking faults, their arrangement and the related long range stresses. Making use of intense synchrotron radiation, (M)XPA allows for unique experiments with high time and space resolution, i.e. in-situ deformation and/or heating studies of the evolution

of essential parameters of nanograin structures, and lateral scans for studies of their spatial distribution.

Acknowledgements

The authors are grateful to the Science Foundation of Austria (FWF) and the Hungarian National Science Foundation for financial support, under projects P17095-N02, and OTKA T46990 & OTKA T43247, respectively. Thanks go also to the Austrian Exchange Office OEAD for supporting mutual visits at the authors' institutions within project A30-/2003 in frame of the Scientific Technical Cooperation Austria-Hungary.

REFERENCES

[1] H. Gleiter, P. Marquardt, Z. Metallk. **75**, 263-267 (1984).

[2] H. Gleiter, Progr. Mater. Sci. 33, 223-315 (1989).

[3] U. Erb, A.M. El-Sherik, G. Palumbo, K.T. Aust, Nanostr.Mater. **2**, 383-390 (1993).

[4] C.C. Koch, Y.S. Cho, Nanostr. Mater. **1**, 207-212 (1992).

[5] J. Eckert, in: Nanostructured Materials — Processing, Properties and Potential Applications, ed. C.C. Koch, Noyes — William Andrew Publ. (Norwich, N.Y., USA), p. 423-526 (2002).

[6] R.Z. Valiev, N.A. Krasilnikov, N.K. Tsenev, Mater.Sci.Eng. A **137**, 35-40 (1991).

[7] R.Z. Valiev, A.V. Korznikov, R.R. Mulyukov, Mater.Sci.Eng. A **168**, 141-148 (1993).

[8] R.Z. Valiev, in: Proc. NATO-ARW Investigations and Applications of SPD, Moscow 1999, Eds. T.C. Lowe and R.Z. Valiev, Kluwer Academic Publishers (2000).

[9] V.M. Segal, V.I. Reznikov, A.E. Dobryshevshiy, V.I. Kopylov, Russian Metallurgy **1**, 99-105 (1981).

[10] R.Z. Valiev, R.Z., I.V. Islamgaliev, I.V. Alexandrov, Progr. Mater. Sci. **45**, 103-189 (2000).

[11] Y. Iwahashi, J. Wang, Z. Horita, M. Nemoto, T.G. Langdon, Scripta Mater. **35**, 143-146 (1996).

[12] Y. Beygelzimer, V. Varyukhin, D. Orlov, B. Efros, V. Stolyarov, H. Salimgareyev, in: Proc 2nd International Symposium on Ultrafine Grained Materials, 2002 TMS Annual Meeting, Seattle, USA, Feb. 17-21, 2002, The Minerals, Metals & Materials Society, Warrendale, 43-46 (2002)

[13] D. Glukhov, Russian patent # 21916552, international priority dated 04.04.2001 (PCT/RU/02/00152).

[14] J. Richert, M. Richert, Aluminium **62**, 604-607 (1986).

[15] M. Richert, H.P. Stüwe, M.J. Zehetbauer, J. Richert, R. Pippan, Ch. Motz, E. Schafler, Mater. Sci. Eng. A **355**, 180-185 (2003).

[16] P.W. Bridgman, Studies in Large Plastic Flow and Fracture, McGraw-Hill, New York (1952).

[17] T. Hebesberger, R. Pippan, H.P. Stüwe, in: Proc. 2nd International Symposium on Ultrafine Grained Materials, 2002 TMS Annual Meeting, Seattle, USA, Feb. 17-21, 2002, The Minerals, Metals & Materials Society, Warrendale,. 133-140 (2002).
[18] S. Erbel, Metals Technology **6**, 482-486 (1979).
[19] M. Zehetbauer, H.P. Stüwe, A. Vorhauer, E. Schafler, J. Kohout, Adv.Eng.Mater. 5, 330-337 (2003).
[20] B.E. Warren, B.L. Averbach, J. Appl. Phys. **23**, 497 (1952).
[21] T. Ungár, A. Borbély, Appl. Phys. Letters **69**, 3173-3175 (1996).
[22] T. Ungár, S. Ott, P.G. Sanders, A. Borbély, J.R. Weertman, Acta Mater. **10**, 3693-3699 (1998).
[23] M. Wilkens, M., in: Fundamental Aspects of Dislocation Theory, ed. J. A. Simmons, R. de Wit, R. Bullough, Vol. . Nat. Bur. Stand. (US) Spec. Publ. No. 317, Washington, DC. USA, 1195-1221 (1970).
[24] M.A. Krivoglaz, in: X-ray and Neutron Diffraction in Nonideal Crystals, Springer Verlag, Berlin, Heidelberg, New York (1996).
[25] G. Cagliati, A. Paletti, F.P. Ricci, Nucl. Instrum. **3**, 223-228 (1958).
[26] P. Klimanek, R. Kuzel Jr., J. Appl. Cryst. **21**, 59-66 (1988).
[27] T. Ungár, I. Dragomir, A. Révész, A. Borbély, J. Appl. Cryst. **32**, 992-1002 (1999).
[28] I. Dragomir, T. Ungár, J. Appl. Cryst. **35**, 556-564 (2002).
[29] R.E. Dinnebier, R. Von Dreele, P.W. Stephens, S. Jelonek, J. Sieler, J. Appl. Cryst. **32**, 761-769 (1999).
[30] A.R. Stokes, A.J.C. Wilson, Proc. Phys. Soc. London **56**, 174-181 (1944).
[31] P.W. Stephens, J. Appl. Cryst, **32**, 281-288 (1999).
[32] B.E. Warren, Progr. Metal Phys. **8**, 147-202 (1959).
[33] C.E. Krill, R. Birringer, Phil. Mag. A **77**, 621-640 (1998).
[34] W.C. Hinds, W. C. Aerosol Technology: Properties, Behavior and Measurement of Airbone Particles, Wiley, New York (1982).
[35] H. Mughrabi, Acta metall. **31**, 1367-1379 (1983).
[36] T. Ungár, I. Groma, M. Wilkens, J. Appl. Cryst. **22**, 26-34 (1989).
[37] G. Ribárik, T. Ungár, J. Gubicza, J. Appl. Cryst. **34**, 669-676 (2001).
[38] K. Levenberg, Quart. Appl. Math. **2**, 164-168 (1944).
[39] D.W. Marquardt, J. Appl. Math. **11**, 431-441 (1963).
[40] E. Tóth-Kádár, I. Bakonyi, L. Pogány, A. Cziráki, Surf Coat. Technol. **88**, 57-65 (1996).
[41] T. Ungár, A. Révész, A. Borbély, J. Appl. Cryst. **31**, 554-558 (1998).
[42] A. Dubravina, M. Zehetbauer, E. Schafler, I. Alexandrov, Mater.Sci.Eng. A **387-389**, 817-821 (2004).
[43] E. Schafler, A. Dubravina, B. Mingler, H.P. Karnthaler, M. Zehetbauer, in: Proc. 3rd Int. Conf. On Nanomaterials by Severe Plastic Deformation — NanoSPD3, Sept. 21-26 (2005), Fukuoka, Japan, ed. Z. Horita, T.C. Langdon, Mater.Sci.Forum, accepted for publication.
[44] M. Zehetbauer, Acta Metall.Mater. **41**, 589-599 (1993).
[45] P. Les, M. Zehetbauer, Key Eng.Mater. **97-98**, 335-340 (1994).
[46] E. Schafler, K. Simon, S. Bernstorff, P. Hanák, G. Tichy, T. Ungár, M.J. Zehetbauer, Acta Mater. **53**, 315-322 (2005).

[47] T. Ungar, M. Zehetbauer, Scripta Mater. **35**, 1467-1473 (1996).
[48] M. Zehetbauer, T. Ungar, R. Kral, A. Borbely, E. Schafler, B. Ortner, H. Amenitsch, S. Bernstorff, Acta Mater. **47**, 1053-1061 (1999).
[49] M. Zehetbauer, E. Schafler, T. Ungar, I. Kopacz, S. Bernstorff, J.Eng.Mater.Techn. ASME **124**, 41-47 (2002).

Received: 21 May 2005.